Journal of Alloys and Compounds 509 (2011) L216–L220

Contents lists available at ScienceDirect

Journal of Alloys and Compounds

journal homepage: www.elsevier.com/locate/jallcom

Letter

Preparation of Fe_2O_3/graphene composite and its electrochemical performance as an anode material for lithium ion batteries

Gang Wang[a], Ting Liu[a], Yongjun Luo[a], Yan Zhao[b], Zhaoyu Ren[b], Jinbo Bai[c], Hui Wang[a,*]

[a] Key Laboratory of Synthetic and Natural Functional Molecule Chemistry (Ministry of Education), College of Chemistry & materials science, Northwest University, Xi'an 710069, PR China

[b] National Key Laboratory of photoelectric technology and Functional materials (Culture Base), National photoelectric technology and Functional Materials & Application International Cooperation Base, Institute of Photonics & Photon-Technology, Northwest University, Xi'an 710069, PR China

[c] Lab. MSS/MAT, CNRS UMR 8579, Ecole Centrale Paris, 92295 Chatenay Malabry, France

ARTICLE INFO

Article history:
Received 26 September 2010
Received in revised form 23 March 2011
Accepted 28 March 2011
Available online 5 April 2011

Keywords:
Iron oxide
Graphene nanosheets
Anode material
Lithium ion batteries

ABSTRACT

The micro-sized sphere Fe_2O_3 particles doped with graphene nanosheets were prepared by a facile hydrothermal method. The obtained Fe_2O_3/graphene composite as the anode material for lithium ion batteries showed a high discharge capacity of 660 mAh g^{-1} during up to 100 cycles at the current density of 160 mA g^{-1} and good rate capability. The excellent electrochemical performance of the composite can be attributed to that graphene served as dispersing medium to prevent Fe_2O_3 microparticles from agglomeration and provide an excellent electronic conduction pathway.

1. Introduction

As the major anode material of commercial lithium-ion batteries (LIBs), graphite has excellent electrochemical properties like charge/discharger reversibility, low and flat working potential similar to that of lithium metal. However, it has a low theoretical capacity about 372 mAh g^{-1}, which terribly affect the performance of LIBs. To meet the increasing demand for LIBs with higher energy density, various attempts to explore new electrode materials have been investigated. Recently, transition metal oxides have been studied as alternative anode materials for LIBs due to their high Li-storage capacities [1–10]. Among the various transition metal oxides, Fe_2O_3 has attracted significant research attention due to its fascinating properties such as the high theoretical capacity (1005 mAh g^{-1}), low cost and low environmental impact [11–13]. However, Fe_2O_3 actually suffer from poor cycle performance when used as the anode material for LIBs. The reason is that the agglomerations and the huge volume change of Fe_2O_3 often occurred during the lithium insertion/extraction process. Up to now, various attempts to overcome the disadvantages of Fe_2O_3 materials have been reported. One of the efficient way is to dope carbonaceous materials with Fe_2O_3, which may buffer the volume expansion and thus improve the electrichemical properties of Fe_2O_3 [14–18].

Graphene, a new crystalline form of carbon, has attracted tremendous scientific interest in both the fundamental and the applied area since it was discovered [19]. It is a very potential material for applications in many technological fields such as nanoelectronics [20], sensors [21], batteries [22] and supercapacitors [23]. Graphene not only possesses stable structure but also high specific surface area, and excellent electronic conductivity. These properties make graphene or graphene-based materials very promising for use as anode materials for reversible lithium storage in LIBs [24]. Although many graphene-based materials as anode materials for LIBs have been reported (Fe_3O_4, TiO_2, SnO_2, Co_3O_4, Mn_3O_4, CuO) [25–31], there are few reports devoted to the simple production of Fe_2O_3/graphene composite. Herein, we reported the facile synthesis of Fe_2O_3/graphene composite. The electrochemical performance of the as-obtained Fe_2O_3/graphene composite as an anode material for LIBs was investigated and compared with pure graphene and Fe_2O_3 electrode.

2. Experimental

Graphene nanosheets were prepared via the H_2 reduction of exfoliated graphite oxide materials at 500 °C. In a typical synthesis of Fe_2O_3/graphene composite, 0.003 mol $FeCl_3 \cdot 6H_2O$, 0.001 mol ascorbic acid, 0.015 g PEG-6000 and 0.6 g urea were dissolved in deionized water (25 ml). The precursor solution was magnetically stirred for 0.5 h. Afterwards 50 mg graphene nanosheets was dispersed in the above solution by ultrasonication for 0.5 h and stirred for another 0.5 h. The mixture was

* Corresponding author. Tel.: +86 29 8836 3115; fax: +86 29 8830 3798.
E-mail address: huiwang@nwu.edu.cn (H. Wang).

0925-8388/$ – see front matter © 2011 Elsevier B.V. All rights reserved.
doi:10.1016/j.jallcom.2011.03.151

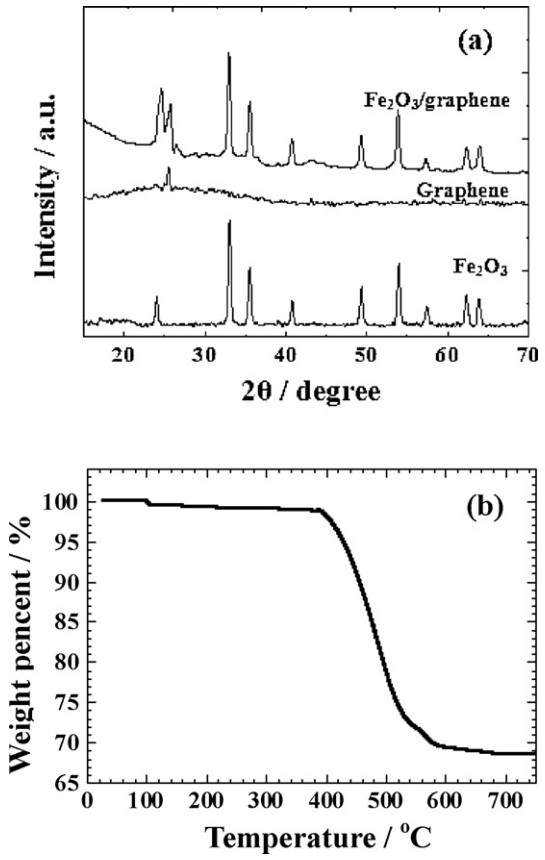

Fig. 1. (a) XRD patterns of Fe_2O_3, graphene and Fe_2O_3/graphene and (b) TGA curve of Fe_2O_3/graphene composite.

then transferred into a 50 ml Teflon-lined autoclave, sealed and maintained at 120 °C for 12 h and then cooled to room temperature naturally. The resulting black solid products were collected by centrifugation, washed with deionized water and dried in vacuum at 80 °C for 12 h. For comparison, we also synthesize Fe_2O_3 microparticles following the same procedure except that no graphene nanosheets were added.

The as-prepared samples were characterized by X-ray diffraction (XRD, Rigaku) and field emission gun scanning electron microscopy (FEG-SEM, JEOL JSM6700 F). High-resolution transmission electron microscope (HRTEM, JEOL JEM-3010) analysis was performed to determine the structural characteristics of the composite on the nanometer domain. Thermogravimetry analysis (TGA) data of the composite were collected in a NETZSCH STA 449C instrument. The sample was heated from 25 to 750 °C in air, and the heating rate was 10 °C/min. The electrochemical testing of the Fe_2O_3/graphene composite was conducted by assembling CR2430 coin cells. The cells were galvanostatically charged and discharged at a current density of 160 mA g^{-1}. The AC impedance spectra of the cells were measured on an electrochemical workstation (CHI 660D) with the frequency range from 0.01 Hz to 100 kHz.

3. Results and discussion

Fig. 1(a) shows the XRD pattern of the Fe_2O_3/graphene composite, in which the diffraction patterns of the pure Fe_2O_3 and graphene nanosheets were also provided for comparison. As shown in Fig. 1(a), the Fe_2O_3/graphene composite possess a weak diffraction at $2\theta = 25.6°$, which assigned to the crystal planes of graphene. The other Nine sharp diffraction peaks at 24.2°, 33.2°, 35.6°, 40.9°, 49.5°, 54.1°, 57.6°, 62.4°, 64.0° correspond well with the crystal planes of (0 1 2), (1 0 4), (1 1 0), (1 1 3), (0 2 4), (1 1 6), (0 1 8), (2 1 4) and (3 0 0) of Fe_2O_3, which can be easily indexed to hexagonal α-Fe_2O_3 (JCPDS 33-0664). The XRD result indicates that the Fe_2O_3/graphene composite is composed of Fe_2O_3 and graphene nanosheets and maintains the crystalline structure of Fe_2O_3 and graphene. The content of graphene nanosheets in Fe_2O_3/graphene composite was quantitatively determined by TGA. Fig. 1(b) shows the TGA curve of the composite. As can be seen from it, the weight loss over the temperature range from 25 to 150 °C is about 1%. This might be due to the loss of residual water in the sample. The weight loss between 350 and 550 °C is about 30%, which represents the amount of graphene nanosheets.

Fig. 2(a) displays the SEM image of Fe_2O_3 microparticles. The sample was almost composed of spherical Fe_2O_3 which agglomerated together with an average diameter of about 2–5 μm and the surface of particle was uneven. From Fig. 2(b), it can be clearly seen that the graphene nanosheets synthesized were composed of randomly aggregated, thin and wrinkled sheets loosely associated with one another. Fig. 2(c) shows the morphology of the Fe_2O_3/graphene composite. The Fe_2O_3 microparticles were randomly doped with graphene nanosheets and the agglomeration of Fe_2O_3 was adequately prevented by these nanosheets. Fig. 2(d) gives a high magnification SEM image of the selected area in Fig. 2(c). A single Fe_2O_3 particle with an uneven surface could be clearly observed, which displayed similar morphology to the pure Fe_2O_3 samples in Fig. 2(a). TEM measurement was performed to identify the number of layers of graphene nanosheets synthesized (Fig. 2(e)). The stacking sheet structure and individual monolayers of graphene could be clearly observed from the inset HRTEM image of the selected area. It is found that the graphene platelet thickness ranged from 3 to 5 nm, which corresponds to an approximately 9–15 layer stacking of the monoatomic graphene sheets. Fig. 2(f) shows the TEM image of Fe_2O_3/graphene composite, the dark area in this figure is part of a Fe_2O_3 microparticle, and the stacking sheets are graphene nanosheets. The inset in Fig. 2(f) displays the atomic resolution HRTEM image of the selected area, in which the (1 0 4) crystal plane of the Fe_2O_3 structure can be clearly identified from the interplanar distances of 0.27 nm.

The electrochemical performance of Fe_2O_3/graphene composite as anode was examined through galvanostatic charge/discharge cycling in the potential range from 0.005 V to 3.0 V vs. Li^+/Li reference electrode. For comparison, the anodic properties of pure graphene and Fe_2O_3 micro particles were also tested under the same conditions. The charge/discharge voltage profiles of the Fe_2O_3/graphene electrode are shown in Fig. 3(a). As can be seen in Fig. 3(a), the voltage profiles of the Fe_2O_3/graphene electrode show a long voltage plateau appears at about 0.8 V during the first discharge process which disappears in the subsequent cycles. The discharge plateau in the galvanostatic curve can be attributed to the electrochemical reaction between the electrode and lithium. As for the electrochemical performance, the Fe_2O_3/graphene electrode exhibits a discharge capacity of 1800 mAh g^{-1} and charge capacity of 1420 mAh g^{-1} in the first cycle, corresponding to a coulombic efficiency of 78%. The irreversible capacity of Fe_2O_3/graphene electrode at the first cycle is mainly attributed to the formation of solid electrolyte interface and the reaction of lithium ion with oxygen containing functional groups [32]. Fig. 3(b) compares the cycling behaviors of Fe_2O_3, graphene and Fe_2O_3/graphene electrodes at the current density of 160 mA g^{-1}. It is clear that much better cycling performance was obtained for the Fe_2O_3/graphene electrode. The discharge capacity after 100 cycles for the Fe_2O_3/graphene electrode is 660 mAh g^{-1}, much higher than that of the Fe_2O_3 (450 mAh g^{-1}) or graphene electrode (550 mAh g^{-1}). The result suggests that Fe_2O_3 microparticles can accommodate extra Li ions when doped with graphene nanosheets. NuLi et al. [33] reported the synthesis of submicron-sized Fe_2O_3 flowers and investigated their electrochemical performance as anode for LIBs. The results revealed that the material could provide a discharge capacity of ~420 mAh g^{-1} after 50 cycles at a current density of 80 mA g^{-1}. Morimoto et al. [34] synthesized micrometric Fe_2O_3 particles by mechanically milling FeOOH at room temperature in air and evaluated their characteristics as lithium intercalation materials. However, the cycle performance was very poor (~200 mAh g^{-1}

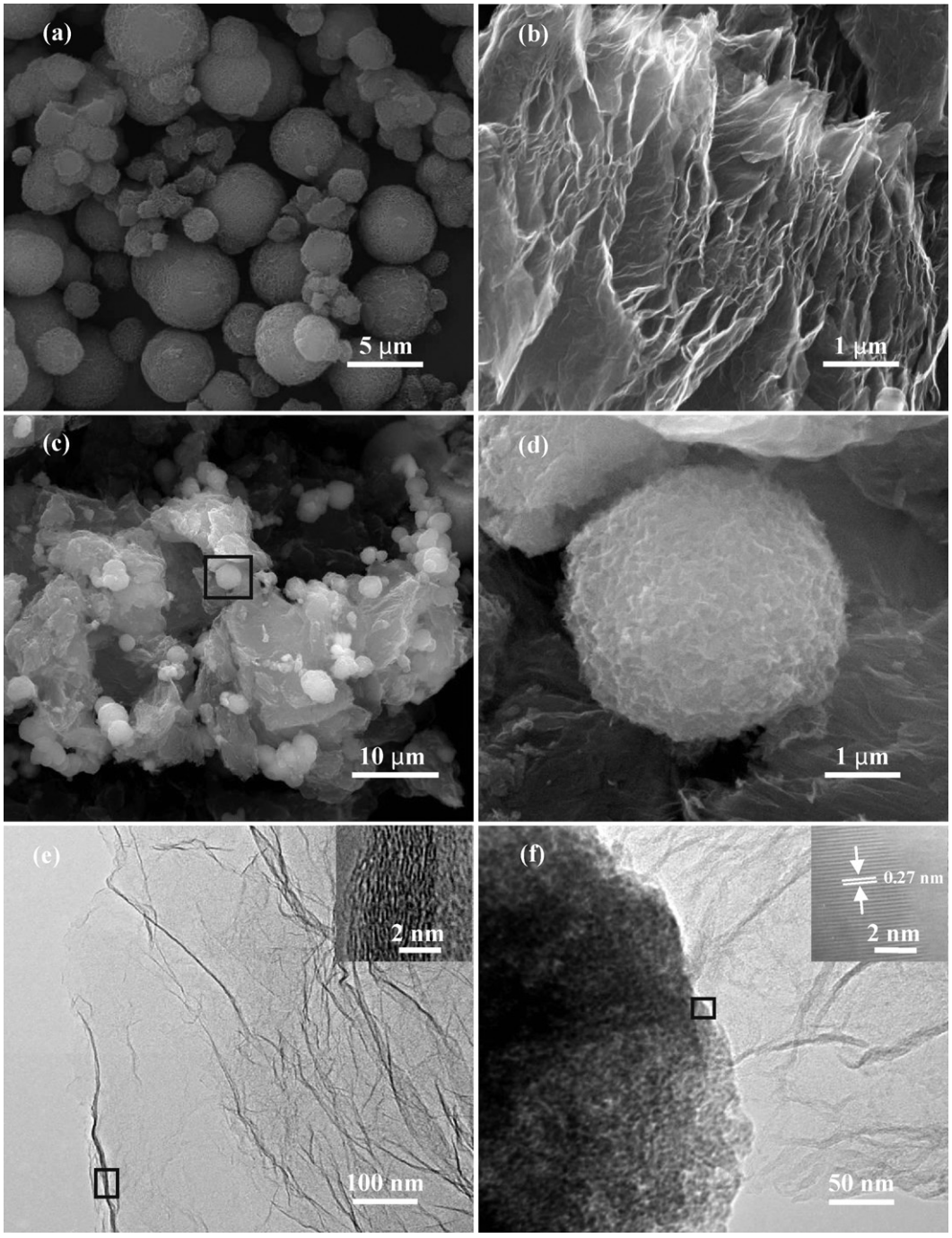

Fig. 2. (a) SEM image of Fe_2O_3 microspheres. (b) SEM image of graphene nanosheets. (c) SEM image of Fe_2O_3/graphene composite. (d) High magnification SEM image of Fe_2O_3/graphene composite of the selected area in Fig. 2(c). (e) TEM image of graphene nanosheets, inset of (e): HRTEM image of graphene nanosheets of the selected area. (f) TEM image of Fe_2O_3/graphene composite, inset of (d): HRTEM image of Fe_2O_3.

after 20 cycles at a current density of 0.5 mA cm^{-2}) as an electrode for LIBs. Our experimental results showed that Fe_2O_3/graphene composite could exhibit an enhanced electrochemical performance at a higher current density of 160 mA g^{-1}, which was much greater than reported data. Fig. 3(c) presents the rate performance of the Fe_2O_3/graphene electrode in comparison with the Fe_2O_3 and graphene electrodes. The current densities used were 160, 400, 800, 1600 and 2400 mA g^{-1}. As can be seen in Fig. 3(c), the Fe_2O_3/graphene electrode shows rather good rate capability with an average discharge capacity of 1108 mAh g^{-1} at the current of 160 mA g^{-1}, 702 mAh g^{-1} at 400 mA g^{-1}, 512 mAh g^{-1} at 800 mA g^{-1}, 463 mAh g^{-1} at 1600 mA g^{-1}, and 322 mAh g^{-1} at 2400 mA g^{-1}, respectively. All of these values are higher than the capacity of Fe_2O_3 or graphene electrodes at the same current densities.

In order to verify that the graphene is responsible for the good performance of the cell with the Fe_2O_3/graphene anode and further compare the electrochemical properties of the different electrodes, the Nyquist plots of the AC impedance for the Fe_2O_3 microparticles and Fe_2O_3/graphene composite were measured after the first charge/discharge cycle (Fig. 4). From Fig. 4, it could be clearly seen that the impedance spectra are almost similar in shape, composed of two semicircles at high- and medium-frequency ranges and followed by a linear part at the low frequency end. The semicircle

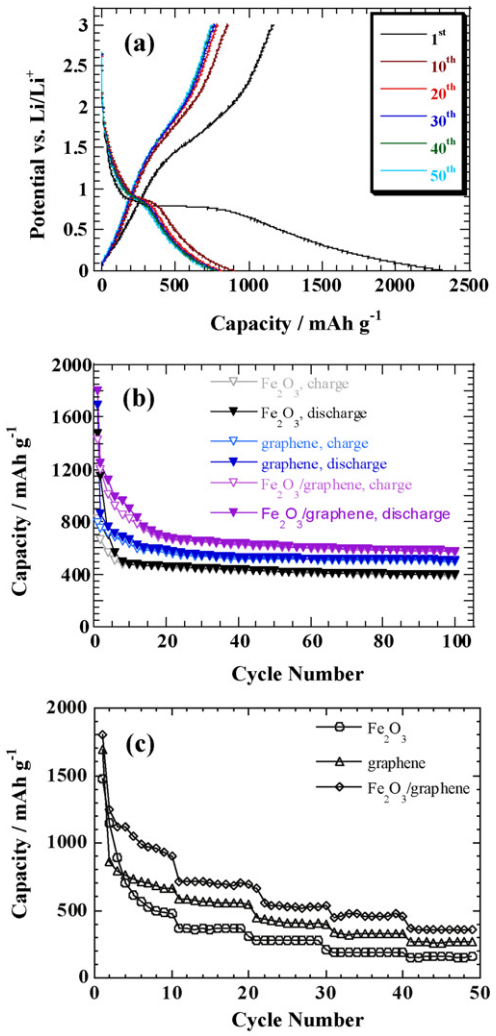

Fig. 3. (a) Charge/discharge profiles of Fe_2O_3/graphene composite electrode. (b) Cyclic performance of the Fe_2O_3, graphene and Fe_2O_3/graphene electrodes cycled between 0.005 and 3.0 V at a current density of 160 mA g^{-1}. (c) Comparison of rate capability of the Fe_2O_3, graphene and Fe_2O_3/graphene electrodes with a charge/discharge specific current range from 160, 400, 800, 1600 to 2400 mA g^{-1}.

in the medium-frequency region is assigned to the charge transfer resistance, which is a measure of the charge transfer kinetics. It is obviously seen from Fig. 4 that the size of the semicircle on the Fe_2O_3/graphene electrode is much smaller than that of the Fe_2O_3 electrode, indicating lower charge transfer resistance. The

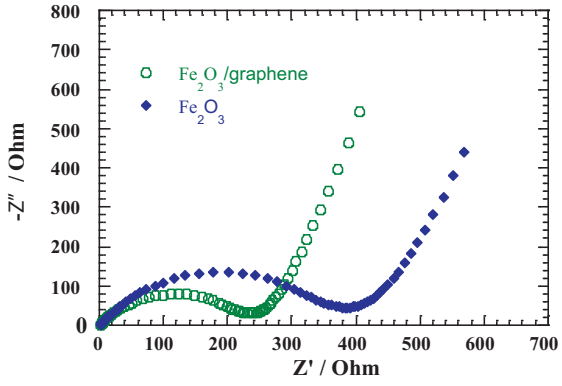

Fig. 4. The impedance plots of the Fe_2O_3 and Fe_2O_3/graphene electrodes.

result indicates that the incorporation of graphene had improved the electronic conductivity, and thus improved the cycling performance. Additionally, the introduction of graphene nanosheets also has a variety of other favorable properties. It is well known that graphene possesses capacities to store lithium ion. Therefore, graphene nanosheets may contribute to the overall capacity of the composite electrode. Furthermore, the agglomeration of Fe_2O_3 microparticles was minimized after doped with graphene nanosheets, which provide sufficient contact area for the reaction of lithium intercalation to Fe_2O_3.

4. Conclusions

Fe_2O_3/graphene composite was synthesized successfully by a hydrothermal method. The electrochemical measurements showed that the Fe_2O_3/graphene electrode presented a higher reversible capacity (660 mAh g^{-1} after 100 cycles at a current density of 160 mA g^{-1}), superior cycle performance compared with the Fe_2O_3 and graphene electrodes. Moreover, the Fe_2O_3/graphene composite described in the present work also shows high rate capability. It can be easily extend this synthetic method to the preparation of other graphene-based materials, which could be used as anode materials for LIBs.

Acknowledgements

The project was supported by the financial supports of the International cooperation research program of National Natural Science Foundation of China (No. 21061130551), the National Basic Research Program of China (973 Program) (No. 2009CB626611), the Ph. D. Programs Foundation of Ministry of Education of China (No. 20096101110002), the National Natural Science Foundation of China (Nos. 20873099 and 10974152), NWU Doctorate Dissertation of Excellence Funds (No. 09YYB04), and National Innovation Experiment Program For University Students (091069710).

References

[1] C.H. Chen, B.J. Hwang, J.S. Do, J.H. Weng, M. Venkateswarlu, M.Y. Cheng, R. Santhanam, K. Ragavendran, J.F. Lee, J.M. Chen, D.G. Liu, Electrochem. Commun. 12 (2010) 496–498.
[2] L.B. Chen, N. Lu, C.M. Xu, H.C. Yu, T.H. Wang, Electrochim. Acta 54 (2009) 4198–4201.
[3] J. Zhong, X.L. Wang, X.H. Xia, C.D. Gu, J.Y. Xiang, J. Zhang, J.P. Tu, J. Alloys Compd. 509 (2011) 3889–3893.
[4] U. Lafont, D. Carta, G. Mountjoy, A.V. Chadwick, E.M. Kelder, J. Phys. Chem. C 114 (2010) 1372–1378.
[5] S. Wang, J. Zhang, C. Chen, J. Power Sources 195 (2010) 5379–5381.
[6] X. Guan, L. Li, G. Li, Z. Fu, J. Zheng, T. Yan, J. Alloys Compd. 509 (2011) 3367–3374.
[7] S. Zhan, Y. Wei, X. Bie, C. Wang, F. Du, G. Chen, F. Hu, J. Alloys Compd. 502 (2010) 92–96.
[8] C. Cai, D. Guan, Y. Wang, J. Alloys Compd. 509 (2011) 909–915.
[9] F. Wu, X. Li, Z. Wang, H. Guo, L. Wu, X. Xiong, X. Wang, J. Alloys Compd. 509 (2011) 3711–3715.
[10] Y.J. Kim, M.S. Park, H.J. Sohn, H. Lee, J. Alloys Compd. 509 (2011) 4367–4371.
[11] H. Liu, G. Wang, J. Park, J. Wang, H. Liu, C. Zhang, Electrochim. Acta 54 (2009) 1733–1736.
[12] L.C. Yang, Q.S. Gao, Y.H. Zhang, Y. Tang, Y.P. Wu, Electrochem. Commun. 10 (2008) 118–122.
[13] H. Liu, D. Wexler, G. Wang, J. Alloys Compd. 487 (2009) L24–L27.
[14] Z. Zhou, Y. Xu, M. Hojamberdiev, W. Liu, J. Wang, J. Alloys Compd. 507 (2010) 309–311.
[15] L.C. Yang, W.L. Guo, Y. Shi, Y.P. Wu, J. Alloys Compd. 501 (2010) 218–220.
[16] Z. Zhou, Y. Xu, W. Liu, L. Niu, J. Alloys Compd. 493 (2010) 636–639.
[17] X. Yang, P. Zhang, Z. Wen, L. Zhang, J. Alloys Compd. 496 (2010) 403–406.
[18] B.T. Hang, S. Okada, J.I. Yamaki, J. Power Sources 178 (2008) 402–408.
[19] B. Banov, L. Ljutzkanov, I. Dimitrov, A. Trifonova, H. Vasilchina, A. Aleksandrova, A. Mochilov, B.T. Hang, S. Okada, J.I. Yamaki, J. Nanosci. Nanotechnol. 8 (2008) 591–594.
[20] P. Blake, P.D. Brimicombe, R.R. Nair, T.J. Booth, D. Jiang, F. Schedin, L.A. Ponomarenko, S.V. Morozov, H.F. Gleeson, E.W. Hill, A.K. Geim, K.S. Novoselov, Nano Lett. 8 (2008) 1704–1708.
[21] Y.H. Zhang, Y.B. Chen, K.G. Zhou, C.H. Liu, J. Zeng, H.L. Zhang, Y. Peng, Nanotechnology 20 (2009) 185504.

[22] E. Yoo, J. Kim, E. Hosono, H. Zhou, T. Kudo, I. Honma, Nano. Lett. 8 (2008) 2277–2282.
[23] M.D. Stoller, S.J. Park, Y.W. Zhu, J.H. An, R.S. Ruoff, Nano. Lett. 8 (2008) 3498–3502.
[24] C. Wang, D. Li, C.O. Too, G.G. Wallace, Chem. Mater. 21 (2009) 2604–2606.
[25] Y.J. Mai, X.L. Wang, J.Y. Xiang, Y.Q. Qiao, D. Zhang, C.D. Gu, J.P. Tu, Electrochim. Acta 56 (2011) 2306–2311.
[26] H. Kim, D.H. Seo, S.W. Kim, J. Kim, K. Kang, Carbon 49 (2011) 326–332.
[27] X. Wang, X. Zhou, K. Yao, J. Zhang, Z. Liu, Carbon 49 (2011) 133–139.
[28] G. Zhou, D.W. Wang, F. Li, L. Zhang, N. Li, Z.S. Wu, L. Wen, G.Q. Lu, H.M. Cheng, Chem. Mater. 22 (2010) 5306–5313.
[29] H. Wang, L.F. Cui, Y. Yang, H.S. Casalongue, J.T. Robinson, Y. Liang, Y. Cui, H. Dai, J. Am. Chem. Soc. 132 (2010) 13978–13980.
[30] D. Wang, D. Choi, J. Li, Z. Yang, Z. Nie, R. Kou, D. Hu, C. Wang, L.V. Saraf, J. Zhang, I.A. Aksay, J. Liu, ACS Nano 3 (2009) 907–914.
[31] X. Shen, J. Wu, S. Bai, H. Zhou, J. Alloys Compd. 506 (2010) 136–140.
[32] X.H. Huang, J.P. Tu, C.Q. Zhang, J.Y. Xiang, Electrochem. Commun. 9 (2007) 1180–1184.
[33] Y. NuLi, P. Zhang, Z. Guo, P. Munroe, H. Liu, Electrochim. Acta 53 (2008) 4213–4218.
[34] H. Morimoto, S. Tobishima, Y. Iizuka, J. Power Sources 146 (2005) 315–318.